Available online at www.sciencedirect.com
ScienceDirect
Journal of Molecular Graphics and Modelling 26 (2008) 1091–1103
Journal of Molecular Graphics and Modelling
www.elsevier.com/locate/JMGM

On the structure, interactions, and dynamics of bound VEGF

Bruno Araújo Cautiero Horta *, José Jair Vianna Cirino, Ricardo Bicca de Alencastro

Physical Organic Chemistry Group, Departamento de Química Orgânica, Instituto de Química, Universidade Federal do Rio de Janeiro, Cidade Universitária, CT, Bloco A, Laboratory 609, Rio de Janeiro, RJ 21941-909, Brazil

Received 10 September 2007; received in revised form 2 October 2007; accepted 2 October 2007
Available online 5 October 2007

Abstract

The vascular endothelial growth factor (VEGF) is believed to be the most important protein in the regulation of the angiogenic cascade. Thus, exploring the structure and dynamical properties of this growth factor and the influence of receptor and inhibitor binding to these properties may reveal new insights on VEGF's biological process and inhibition opportunities. Here we describe an analysis of molecular dynamics simulations of VEGF bound to the Flt-1 receptor, VEGF bound to the v107 peptide inhibitor, and also VEGF bound to a mutant v107. We analyze the effects of binding to VEGF regarding three aspects: structure, interactions, and dynamics. We found that the structure of VEGF is not significantly perturbed upon binding. We analyze the individual contribution of the VEGF residues to the total interaction energy of binding to Flt-1 and v107. We also compare dynamical variables such as thermal fluctuations and correlations with those of the unbound form. We found that receptor binding is able to promote stronger perturbations on the VEGF dynamical behavior than VEGF inhibitor binding. VEGF motions in the receptor bound complex are shown to be less correlated than motions of unbound VEGF. The work addresses the changes on conformational flexibility of the isolated VEGF upon binding, as well as changes in structure and side-chain rearrangements.

Keywords: VEGF; Angiogenesis; Molecular dynamics; Receptor binding; Inhibition; Principal component analysis

1. Introduction

Vascular endothelial growth factors (VEGFs) are the most important and extensively studied angiogenic regulators [1–4]. They are polypeptides that belong to the cystine-knot superfamily of signaling proteins, which, in humans, include platelet derived growth factor (PDGF), placental growth factor (PlGF), vascular endothelial growth factor-A (VEGF-A), VEGF-B, VEGF-C and VEGF-D [5]. Other VEGFs, such as VEGF-E and VEGF-F, are also expressed in other organisms [6]. The members of the VEGF family act by differential activation of three tyrosine kinase receptors: Flt-1 (also known as VEGFR-1), KDR (known as Flk-1 or VEGFR-2) and Flt-4 (VEGFR-3) [7]. These receptors are predominantly expressed in endothelial cells. VEGF-A activates Flt-1 and KDR, PlGF and VEGF-B only activate Flt-1, VEGF-C and VEGF-D activate KDR and Flt-4. Both KDR and Flt-1 are necessary to embryonic development [8]. In adults, KDR seems to be the most important VEGF receptor and its activation promotes endothelial cell migration, *in vivo* angiogenesis and increased vascular permeability. Flt-1 appears to be involved in the monocyte and macrophage migration and the sequestering of excess VEGF-A [9]. Flt-4 is mainly related to the growth of lymphatic vessels, which is known to be associated with the metastatic spread of tumor cells [10,11].

Muller et al. determined the crystal structure of the receptor-binding domain of VEGF-A (VEGF-$A_{8–109}$) (PDB codes: 1VPF and 2VPF), showing that there exists good similarity between the structure of VEGF-A and the structure of the platelet derived growth factor (PDGF) (PDB code: 1PDG) [12,13]. Mutational analysis has revealed that the residues located in the poles of the VEGF-A homodimer predominantly govern the interactions with the receptor KDR [13]. The crystal structure of the complex formed by domain-2 of Flt-1 and the VEGF-A dimer (PDB code: 1FLT) suggested that, for this receptor, the poles of VEGF-A are also responsible for binding and that the interactions are predominantly hydrophobic [14].

Peptides that have high affinity to VEGF and are able to inhibit receptor binding have been synthesized using phage

* Corresponding author. Tel.: +55 21 2562 7132; fax: +55 21 2562 7132.
E-mail addresses: bruno@iq.ufrj.br (B.A.C. Horta), bicca@iq.ufrj.br (R.B. de Alencastro).

1093-3263/$ – see front matter © 2007 Elsevier Inc. All rights reserved.
doi:10.1016/j.jmgm.2007.10.001

display techniques to serve as lead compounds in the design of small molecule inhibitors [15]. The structures of complexes involving VEGF bound to peptides have been described (PDB codes: 1KAT and 1VPP) [16,17].

In a recent work [18], we performed a molecular dynamics (MD) simulation of the unbound VEGF in water. Our results suggest that there exists a certain degree of correlation between the motions of loops-1 and -3, located in the same pole of the dimer. Principal component analysis (PCA) showed as the principal mode (the eigenvector that corresponds to the higher eigenvalue), a type of motion in which the poles are projected one against the other as the wings of a butterfly [18,19]. Evidence of the existence of correlations has arisen from the superposition of structures obtained from a multiple copy X-ray structure and NMR experiments, in which loop-3 appears as a sequence of snapshots of a concerted motion [12,16]. The existence of correlated motions between the residues that form the poles provides a dynamical ground for the intimate activity relationship observed between loops-1 and -3 upon sequence replacement [6,20]. It seems that correlations on the motions of the loops play a certain role on the high affinity receptor binding [18].

The present work aims to investigate the effects of binding on the structure and dynamics of the vascular endothelial growth factor. Three model systems were considered for analysis: (i) the complex formed by VEGF and the receptor Flt-1, (ii) the complex formed by VEGF and the v107 peptide inhibitor and (iii) the complex formed by VEGF and a mutant v107 peptide inhibitor. The work addresses changes on conformational flexibility of the isolated VEGF upon binding, as well as changes in structure and side-chain rearrangements.

2. Methodology

2.1. Initial structures

We have constructed three models (see Table 1): the complex between VEGF and the domain-2 of the VEGFR-1 receptor (VEGF_VEGFR-1_{D2}); the complex between VEGF and the peptide inhibitor V107 (VEGF_v107); and the complex between VEGF and a mutant V107 (VEGF_$v107_{mut}$) in which the residue Glu4 was substituted by an alanine.

The coordinates for the complex VEGF_Flt-1_{D2} were taken from the crystal structure (PDB code: 1FLT) [14]. The refined structure includes residues 13–107 and 12–109 of the two $VEGF_{8–109}$ monomers, and 132–225 and 132–226 of the two copies of Flt-1_{D2}. We have included the terminal residues 11, 12, 108 and 109 on the first monomer, residue 11 on the second monomer of VEGF, and we have also included residue 226 on the first copy of Flt-1_{D2}. These inclusions were performed in order to equate the numbers of residues of the VEGF protein in all models (11–109, the same size that we used on the study of the unbound VEGF) and to equate the number of residues in the receptor copies. The inclusion of these residues was performed using the Sybyl program [21], minimizing each included residue keeping the rest of the protein fixed. The coordinates for the VEGF_v107 complex were taken from the first snapshot of the 1KAT set of NMR structures [16]. In this structure, each VEGF monomer includes residues 11–109 and each copy of v107 inhibitor includes residues 1–19. The VEGF_$v107_{mut}$ was constructed from the VEGF_v107 in which the glutamic acid residue (Glu4) was replaced by an alanine (also using Sybyl). The receptor-binding domain of VEGF in these models includes the same number of residues, 11–109. Initial models are summarized in Table 1.

2.2. Molecular dynamics

Simulations were performed within the NPT ensemble using the GROMACS [22,23] simulation package and the OPLS all-atom force field developed for protein simulations [24]. Energy minimizations using 1000 steps of the steepest descent algorithm were applied in order to remove bad contacts. The minimized systems were solvated using SPC water molecules [25] in rectangular boxes constructed with each edge from at least 9 Å of the protein surface [26]. The systems were neutralized by replacing solvent molecules with counterions [27] using the genion module of GROMACS. The bonds involving hydrogen atoms were constrained using the LINCS algorithm [28]. Periodic boundary conditions (PBC) were applied and the long range electrostatic interactions were treated using the Ewald summation method (PME) [29]. Simulations of the solvent molecules and counterions were performed at 300 K and 1 atm for 40 ps in order to equilibrate them in the field of the potential exerted by the protein and to fill the cavities on the surface of the protein. In this step, the coordinates of the protein atoms were restrained using harmonic potentials. The numerical integration of the equations of motion was performed using the Verlet Leapfrog algorithm [30]. Temperature and pressure were controlled using Berendsen's formalism of weak coupling to external bath and via isotropic coordinate scaling, with relaxation times of 1 and 0.1 ps, respectively; and isothermal compressibility of 4.5 e^{-5} bar^{-1} [31]. The energies of the systems were minimized for 1000 steps of steepest descent. The systems were heated to 300 K using six blocks of calculation in which the temperature

Table 1
Initial models used in the simulations

Model	Source PDB code	VEGF residues per chain	Flt-1_{D2} residues per copy	V107 residues per copy
VEGF_Flt-1_{D2}	1FLT	11–109[a]	132–226[a]	
VEGF_v107	1KAT	11–109		1–19
VEGF_$v107_{mut}$	1KAT	11–109		1–19

[a] After inclusion of mentioned terminal residues to equate the primary sequences of the models.

was gradually increased. Each block lasted 50 ps, totalizing 300 ps of the heating process for each system. The equilibrated systems (300 K and 1 atm) were simulated using a time-step of 0.002 ps until a total time of 10 ns.

2.3. Correlated motions

In order to analyze the effect of binding on the collective motions of the VEGF protein, we have used the same methodology of our previous work [18]. The elements of the dynamical cross-correlation matrix C_{ij} (Eq. (1)), which corresponds to the normalized covariance matrix (c_{ij}), were calculated and analyzed using 2D plots defined as dynamical cross-correlation maps (DCCM). A complete mathematical formalism for obtaining these maps can be found elsewhere [32–34].

$$C_{ij} = \frac{\left\langle \Delta r_i \Delta r_j \right\rangle}{\left\langle \Delta r_i^2 \right\rangle^{1/2} \left\langle \Delta r_j^2 \right\rangle^{1/2}} \quad (1)$$

where Δr_i and Δr_j correspond to the atomic displacement vectors for atoms i and j, respectively, and the angle brackets denote time averages. The dynamical cross-correlation matrices were calculated through the last 5 ns of the simulation as block averages, in which time lengths of 250, 500 and 1000 ps were considered for the size of each block. The results were almost invariant with the size of the block, so we only show the results for the size of 1000 ps. The translational and rotational motions were removed by fitting the structures to the initial structure using the α-carbons of the residues 18–33, 46–58, 68–78, and 90–100 of VEGF as reference. These residues compose the most rigid regions of the protein and were chosen according to the values of the experimental B-factor. The residues with a high B-factor value were not considered for the fitting procedure because the use of residues of regions of high flexibility is usually responsible for the appearance of artificial correlated motions [32]. As we wanted to analyze the effects of binding on the dynamical behavior of VEGF, the maps were constructed using only the residues of VEGF.

2.4. Principal component analysis

The principal component analysis is based on diagonalizing the 3N × 3N covariance matrix of atomic coordinates (Eq. (2)).

$$C = T\Lambda T^{\mathrm{T}} \text{ or } \Lambda = T^{\mathrm{T}} C T \quad (2)$$

In this equation C is the covariance matrix, Λ is the diagonal matrix that includes the eigenvalues ranked by magnitude, and T is the transformation matrix that includes the corresponding eigenvectors. Each eigenvector corresponds to an internal motional mode of the system. The covariance matrix was constructed and diagonalized for the α-carbon atoms of each protein over the last 5 ns of simulation. This was performed with the module ''g_covar'' of the GROMACS simulation package [22]. The first five residues (11–15) and last five residues (105–109) were removed from each monomer to prevent highly flexible terminal motions to dominate the analysis [35]. Translational and rotational motions were removed by least square fitting to the most rigid residues of VEGF (18–33, 46–58, 68–78, and 90–100). Trajectories were projected onto the principal motional modes using the module ''g_anaeig'' implemented in GROMACS [22].

3. Results and discussion

3.1. Stability of the simulations

Fig. 1 shows the RMS deviation from the initial structure, the radius of gyration and the solvent accessible surface area (SASA) for the models considered in this study. RMS deviations from initial structures are stable during the entire simulations and converged to values about 0.2 nm. Radius of gyration and SASA were calculated showing that no significant conformational changes occurred during the simulations.

3.2. Structural analysis

In 1997, Muller et al. revealed the three-dimensional structure of VEGF (PDB codes 1VPF and 2VPF) [12,13]. In the same year, Wiesmann et al. determined the crystal structure of VEGF bound to two copies of the domain two of Flt-1 receptor (PDB code 1FLT) [14]. Interestingly, no significant structural differences were observed between the unbound and bound form of VEGF [14]. Two years later, Starovasnik et al. showed by NMR spectroscopy that the structure of the receptor is also not significantly affected upon binding (PDB code 1QSV) [36]. In 2002, Pan et al. showed by NMR spectroscopy that binding to v107 peptide also does not induce significant changes in the structure of VEGF [16].

Fig. 2 shows the superimposition of the average structures of unbound VEGF, VEGF bound to Flt-1, and VEGF bound to

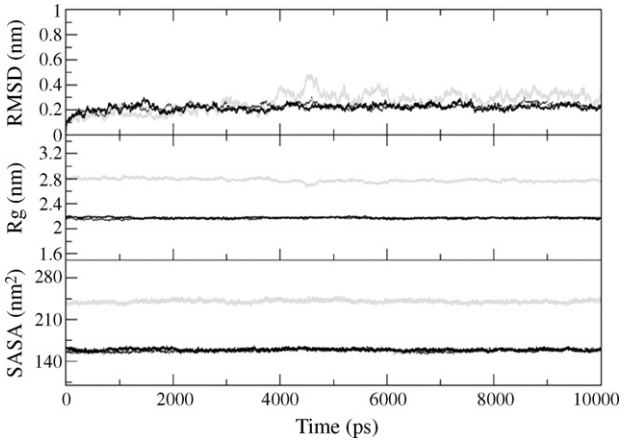

Fig. 1. RMSD of the α-carbon atoms of VEGF_Flt-1_{D2}, VEGF_v107, and VEGF_$v107_{mut}$. The light gray line represents the RMSD of VEGF_Flt-1_{D2}, the black line represents the RMSD of VEGF_v107 and the dotted line represents the RMSD of VEGF_$v107_{mut}$. The average (all direction) radius of gyration and the solvent accessible surface area (SASA) of the same models are also shown using the same representation scheme.

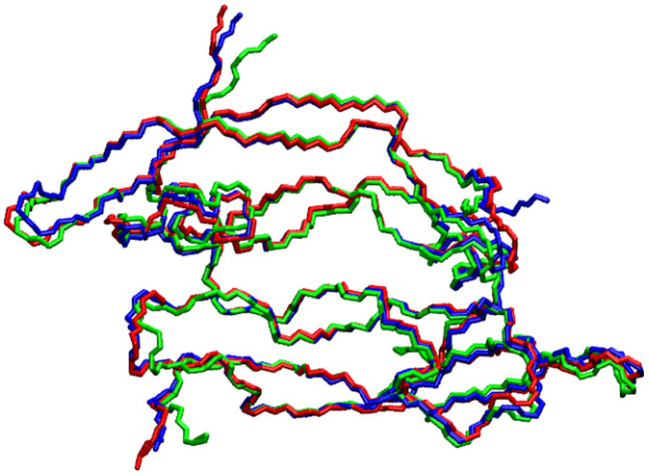

Fig. 2. Superimposition of average structures of unbound VEGF (blue), VEGF bound to Flt-1_{D2} (red), and VEGF bound to v107 (green).

v107. Averaging was performed by fitting 2500 snapshots of the last 5 ns of each trajectory using the α-carbon atoms of the most rigid residues of VEGF (18–33, 46–58, 68–78, and 90–100). RMS deviations with respect to the unbound structure were calculated over all backbone residues showing that the structure of VEGF in complex with Flt-1 (RMSD = 0.95 Å) is more similar to the unbound structure than the structure of VEGF bound to v107 is (RMSD = 1.44 Å). The most apparent differences lie on the terminal and loop residues. Pan et al. showed that the atomic RMSD between the average crystal structures of unbound VEGF (PDB codes: 1VPF and 2VPF) and the average NMR structures of VEGF bound to v107 is 0.87(±0.07) Å for residues 5–105 [16]. Considering the same range of residues the RMSD calculated herein between unbound VEGF and VEGF bound to v107 goes to 0.83 Å, showing excellent agreement with experimental observations. When RMSD is calculated between the crystal structure of VEGF bound to Flt-1 and the average of the same ensemble of unbound crystal structures of VEGF, considering the same residues (5–105), the value of 0.52 Å is obtained, which is comparable to the result of 0.67 Å obtained from the average structures of the simulations. The results above indicate that the structure of VEGF is only slightly perturbed upon binding, as already mentioned by experimentalists. Furthermore, it seems that the small v107 peptide is able to promote larger modifications on VEGF structure if compared to Flt-1 receptor. All RMS deviations were computed using Pro-Fit code [37,38].

The secondary structure of unbound VEGF, VEGF bound to Flt-1, and VEGF bound to v107 was extracted using the STRIDE program [39] for every 10 ps and plotted as a function of time (results not shown). No strong perturbations were identified in the secondary structure of VEGF upon binding. The secondary structure content was obtained by averaging the percentage of each secondary element collected every 2 ps over the last 8 ns of the trajectories (results not shown). The secondary structure content of unbound VEGF is almost identical to that of VEGF bound to Flt-1, but slightly different from that of v107, which shows a 1% higher α-helical content and 1.5% lower β-sheet content.

Table 2
Average number of hydrogen bonds separated by groups

	Unbound VEGF	VEGF bound to Flt-1	VEGF bound to v107
Protein/protein	131.0 ± 4.8	130.5 ± 4.9	126.8 ± 4.8
Main-chain/main-chain	86.1 ± 3.6	84.4 ± 3.6	85.6 ± 3.4
Side-chain/side-chain	22.8 ± 2.3	20.9 ± 2.4	19.4 ± 2.7
Chain-1/chain-2	8.8 ± 1.5	12.4 ± 2.2	7.6 ± 1.4
Chain-1/chain-1	60.4 ± 3.3	59.3 ± 3.2	61.7 ± 3.5
Chain-2/chain-2	61.7 ± 3.4	58.9 ± 3.4	57.5 ± 3.1

Hydrogen bonds were analyzed using the "g_hbond" module of GROMACS package [22]. Table 2 shows the number of hydrogen bonds averaged over 4000 snapshots of the last 8 ns. These numbers were obtained by defining two groups and calculating the existence, or not, of hydrogen bond by following the criteria: (i) cutoff distance between heavy atoms donor and acceptor of 3.5 Å and (ii) cutoff angle acceptor-donor-hydrogen of 30°. The pairs analyzed in the groups were: (i) protein/protein; (ii) main-chain/main-chain; (iii) side-chain/side-chain; (iv) chain-1/chain-2 (inter-chain); (v) chain-1/chain-1; and (vi) chain-2/chain-2. Values indicate that binding to Flt-1 results in a small reduction on the number of side-chain hydrogen bonds and an increase on the number of inter-chain hydrogen bonds. Binding to v107 seems to induce larger alterations in the number of hydrogen bonds. In this case, the total number of hydrogen bonds (protein/protein) is reduced by 4, mainly because of the reduction in the number of side-chain and inter-chain hydrogen bonds.

3.3. Interactions between VEGF and Flt-1_{D2} receptor

Flt-1, as all other VEGF receptors, is composed by seven immunoglobulin-like domains on its extracellular portion. Deletion studies on Flt-1 have shown that domain-2 binds to VEGF only 60-fold less tightly than the full receptor. Domains 2 and 3 together almost recover the binding affinity of the full receptor, indicating that these domains sufficiently account for the interactions with VEGF, and that the other domains must be related to signal transduction [14].

The crystal structure of the complex has revealed that no major conformational changes occur on the structure of VEGF upon binding to Flt-1. Both monomers of VEGF contact each copy of the receptor domain-2. Each copy of the receptor lies on a pole of VEGF and buries approximately 820 $Å^2$ of the total surface area. The contacts between the two copies of the domain-2 of Flt-1 are mainly mediated by hydrophobic interactions [14].

An analysis of the energetic contribution per residue was carried out in order to identify which residues of VEGF contribute more to the total binding energy (Fig. 3A and B). This analysis was performed by averaging the electrostatic and Van der Waals (VdW) contribution per residue of VEGF, treating each residue as a group and computing the interactions between each group and the group formed by the entire receptor. This procedure is based on the partition and summation properties of the parametrized force field and, for this reason, only approximate qualitative assumptions can be

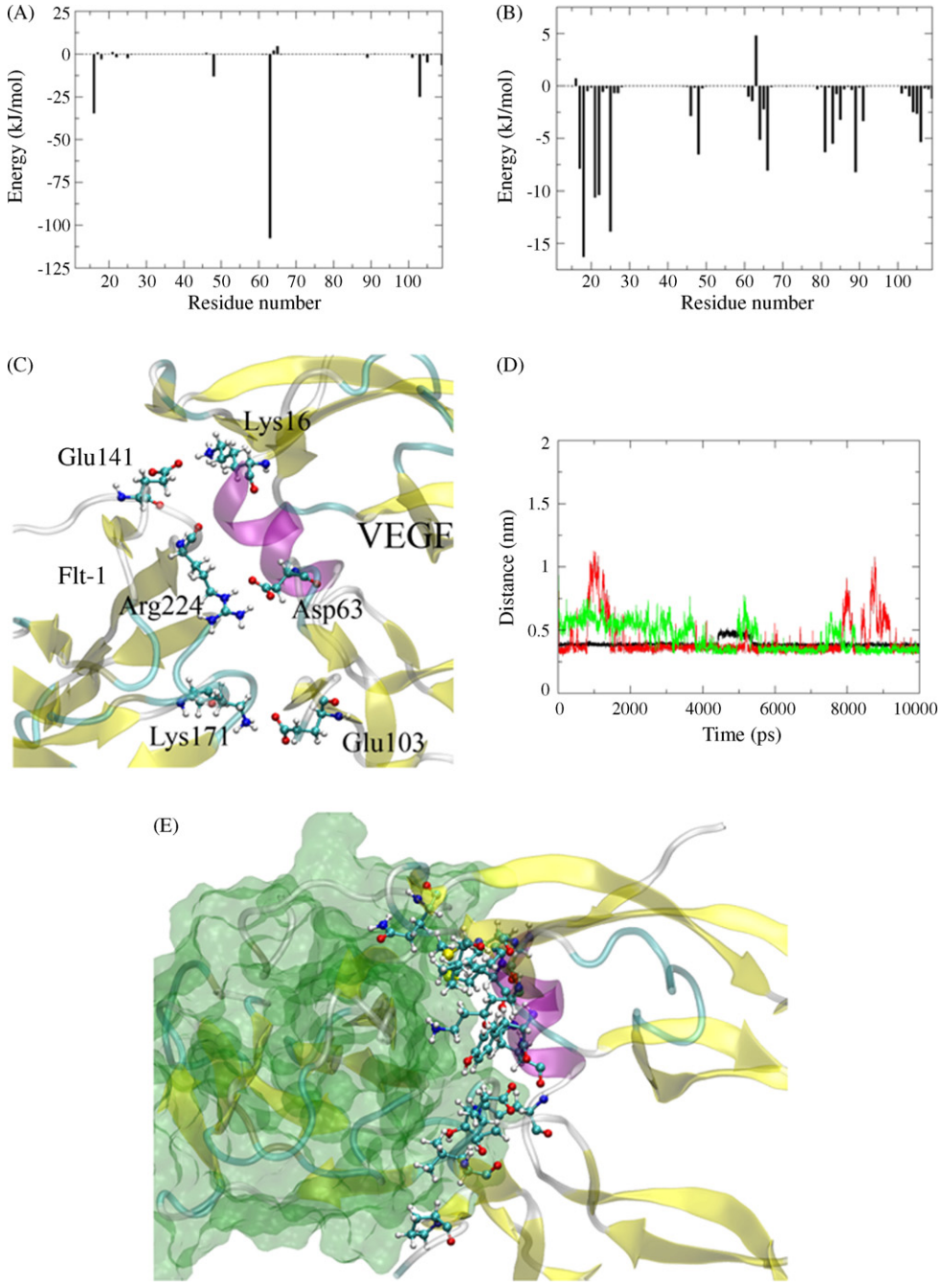

Fig. 3. (A) Electrostatic and (B) VdW contribution per residue of VEGF to the entire Flt-1 group. (C) Charged interactions between VEGF and Flt-1. (D) Distances between the pairs of residues Flt-1-Glu141 and VEGF-Lys16 (red), Flt-1-Arg224 and VEGF-Asp63 (black), and Flt-1-Lys171 and VEGF-Glu103 (green). (E) Residues of VEGF that contribute with more than 5 kJ/mol to the VdW interaction with the group formed by the full Flt-1. Molecular graphics were generated by the use of VMD [42].

extracted. Within the limitations of the method, pairs of residues that contribute to the total binding energy were identified.

Differently from the results described in reference 14 (examination of the crystal structure of the complex), in which only one direct polar interaction was identified (Arg224 of Flt-1 and Asp63 of VEGF) [14], four direct polar interactions were identified between VEGF and Flt-1 using our methodology. In addition to the previously identified interaction between Arg224 of Flt-1 and Asp63 of VEGF, three other interactions were found between the following residues: Flt-1-Lys171 and VEGF-Glu103, Flt-1-Glu141 and VEGF-Lys16, Flt-1-Thr38 and VEGF-Lys48. Except for the last, which is an interaction between the backbone carbonyl oxygen of Thr38 and the positive amino group of Lys48, all other interactions occur between charged side-chains (Fig. 3C). The additional interactions found, although stable (Fig. 3D) are much weaker (Fig. 3A). Mutations of these residues to alanine have shown only a modest decrease in the binding affinity [16,40]. Nevertheless, despite the weakness of these interactions, the

presence of complementary charged pairs may have some effect on receptor selectivity and binding orientation [41].

The non-polar interactions were also analyzed (Fig. 3B). The most significant contributions were due to the residues that are deeply buried in the interface. Fig. 3E shows the residues of VEGF that contribute with more than 5 kJ/mol to the total VdW interaction energy with the group formed by the entire Flt-1. These residues are: Phe17, Met18, Tyr21, Gln22, Tyr25, Lys48, Glu64, Leu66, Met81, Ile83, Gln89 and Pro106.

3.4. Interactions between VEGF and peptide inhibitors

Peptides that have high affinity to VEGF and are able to inhibit receptor binding have been synthesized using phage display techniques [15]. The crystal structure of the complex of VEGF with the v108 peptide (PDB code: 1VPP) was determined. The authors stated that this peptide is not a good lead to the design of new small molecule inhibitors because no specific side-chain interactions to VEGF were found, while only some backbone hydrogen bonds were responsible for the major part of the binding energy [17]. On the other hand, the v107 peptide (PDB code: 1KAT) proved to be a good candidate for small molecule design since the NMR structure of its complex to VEGF shows that this inhibitor binds in the same region of the receptor and maintains specific side-chain contacts. The main interactions found between VEGF and v107 are of hydrophobic nature similarly to those found between VEGF and Flt-1 [16]. v107 is an amphipathic peptide and the structure of the complex shows that the hydrophobic residues are well defined and interacting with the hydrophobic surface of the VEGF-binding site, and that the charged or polar residues have poorly defined and solvent exposed side-chains. As described by Pan et al. the side-chains of v107-Ile7, -Ala8, -Met10, -Trp11, -Trp13, -Phe16 and -Leu19 form a hydrophobic surface that buries the surface formed by VEGF residues Phe17, Met18, Tyr21, Tyr25, Gln22, Tyr25, Lys48, Asn62, Asp63, Leu66, Met81, Ile83 and Cys104. Furthermore, the authors have suggested that v107-Arg9 could potentially form a salt bridge interaction with VEGF-Glu103 [16].

The analysis of the molecular dynamics simulation of the complex VEGF_v107 revealed that, after 6 ns of simulation, the side-chain of v107-Arg9, which was interacting with the side-chain of v107-Glu4, stopped this intramolecular interaction and started to interact with the VEGF-Glu103 side-chain. This interaction remained stable until the end of the simulation, reinforcing the suggestion proposed by the experimentalists.

An analysis of the energy contribution per residue of VEGF was also carried out for the complex with v107. Fig. 4A and B shows the average of the electrostatic and VdW contribution per residue of VEGF. The filled black bars show the interactions before the formation of the salt-bridge between VEGF-Glu103 and v107-Arg9, and the non-filled red bars show the interactions after the salt-bridge formation. In both cases, residues Tyr21 and Asn62 of VEGF contribute significantly to the electrostatic interaction energy. Tyr21 phenol oxygen is hydrogen bonded to the NH backbone of v107-Trp11 while Asn62 amide hydrogen atoms are hydrogen bonded to the backbone carbonyl oxygen atoms of residues Ile7 and Arg9 of v107. Pan et al. have shown that the largest difference between the VEGF_v107 and VEGF_Flt-1_{D2} complex interfaces is due to the conformation of residue Asn62 that, in the case of VEGF_Flt-1_{D2} ($\phi = \sim 52^{\circ}$), points away from the binding site while in the case of VEGF_v107 ($\phi = -76(\pm 9)^{\circ}$), interacts intimately with v107 [16]. Thus, the specific charged interactions found between Asn62 and the backbone of v107 may help to maintain this conformation. In the case of VEGF_Flt-1_{D2}, the presence of hydrophobic side-chains at the interface may be responsible for the positive ϕ angle of Asn62 [14,16]. Experimentalists have also raised the possibility of a flipping process between positive and negative values for the ϕ angle of Asn62 [16], supporting the existence of equilibrium between two backbone conformations of VEGF. This was not observed in the MD simulations, at least during the simulation time (10 ns). Details of the MD simulation of free VEGF can be found elsewhere [18]. The average value of the ϕ angle was $-77(\pm 12)^{\circ}$ for the free VEGF, $-70(\pm 10)^{\circ}$ for the VEGF_v107 complex and $75(\pm 10)^{\circ}$ for the VEGF_Flt-1_{D2} complex. It is possible that the backbone of the free VEGF is in equilibrium between two conformations, or that an induced conformational change is promoted by the fitting of Flt-1_{D2}. Fig. 4A also shows the contribution of residue Glu103 when the salt-bridge is formed (red bars).

In order to release the side-chain of v107-Arg9 to interact with VEGF-Glu103, we also constructed a mutant v107 (VEGF_$v107_{mut}$) in which Glu4 was replaced by an alanine and performed a 10 ns MD simulation. Although the side-chain of v107-Arg9 started to interact with VEGF-Glu103 in the beginning of the simulation (2 ns), this interaction was not as stable as expected (Fig. 4E). One of the reasons for this is that this mutation promotes undesirable conformational changes in the structure of the peptide that disturb the interactions with VEGF. The mutation to alanine has made the surface of the peptide more hydrophobic and, as this position is solvent exposed in the complex, the reorganization may have occurred to increase solvent affinity, but with decreasing VEGF affinity as a side effect. A mutation at this position to positively charged or non-charged polar residues might liberate the side-chain of v107-Arg9 without perturbing the solvation properties so drastically.

Mutational analysis are often performed by experimentalists in order to achieve an approach to the per residue contribution on the total interaction energy. The results above exemplify a situation in which a non-additive contribution to the total energy of binding to VEGF is expected since large conformational changes occur. No experimental data is available for the mutation of the Glu4 residue. However, Pan et al. observed non-additive energy contributions due to the mutations of the hydrophobic residues of v107 which contact VEGF [16]. This indicates that point mutations are affecting deeply the structure of the peptide in the bound state. In the case of the unbound state, the peptide was shown to be poorly structured [16]. Thus, it is difficult to access the effects of point mutations on the structure of the free peptide by experimental ways.

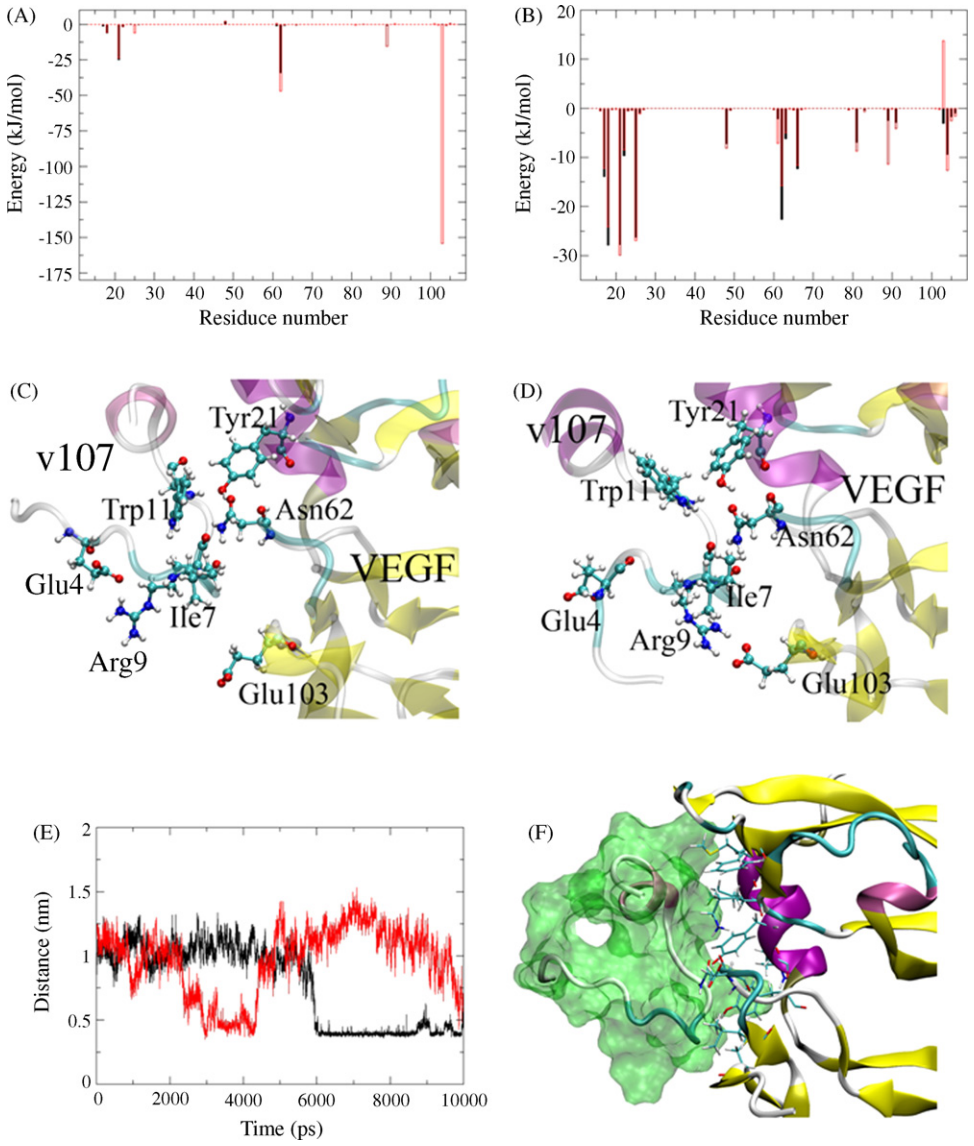

Fig. 4. (A) Electrostatic and (B) VdW contribution per residue of VEGF to the entire v107 group. The filled black bars show the interactions before the formation of the salt-bridge (between VEGF-Glu103 and v107-Arg9) and the non-filled red bars show the same after the salt-bridge formation. (C) Snapshot showing the residues that contribute significantly to the electrostatic interactions between VEGF and v107 before the formation of the salt-bridge and (D) after the formation of the salt-bridge. (E) Distance between v107-Arg9 and VEGF-Glu103; the black line refers to VEGF_v107 and the red line to VEGF_v107$_{mut}$. (F) Residues of VEGF that contribute with more than 5 kJ/mol to the VdW interaction with the group formed by the full v107. Molecular graphics were generated by the use of VMD [42].

The VdW interactions were also analyzed. Fig. 4B shows the residues of VEGF that contribute with more than 5 kJ/mol to the total VdW interaction energy with the group formed by the entire v107 inhibitor. These residues are: Phe17, Met18, Tyr21, Gln22, Tyr25, Lys48, Asn62, Asp63, Leu66, Met81 and Cys104. Our results suggest that Asn62 is also important for the high affinity binding to v107, but no experimental binding affinity estimation is available for this residue.

3.5. Side-chain analysis

Probability distributions along the χ angle were calculated in order to analyze the effects of binding on the side-chains of selected residues of VEGF which are located at the receptor-binding region (Fig. 5). Selected residues are shown in Fig. 3E. In Fig. 5, the black line refers to unbound VEGF, red line to VEGF bound to Flt-1 and the green line corresponds to VEGF bound to v107. Some of these angle distributions are not significantly affected upon binding. This is the case of residues Phe17, Tyr25, Leu66, Met81 and Ile83. In the case of Met18 and Tyr21, it is noticed that distributions are similar between unbound and Flt-1 bound VEGF. Gln22 has a much more localized equilibrium angle in the VEGF bound to Flt-1 system while it has almost the same delocalized behavior in the unbound and VEGF bound to v107. Lys48 and Glu64 appear more localized in the unbound state. Finally, Gln89 and Pro106 represent a situation in which unbound VEGF is similar to VEGF bound to v107 but differs from VEGF bound to Flt-1. Diversity on the orientation of these side-chains may implicate in novel strategies for drug design and docking

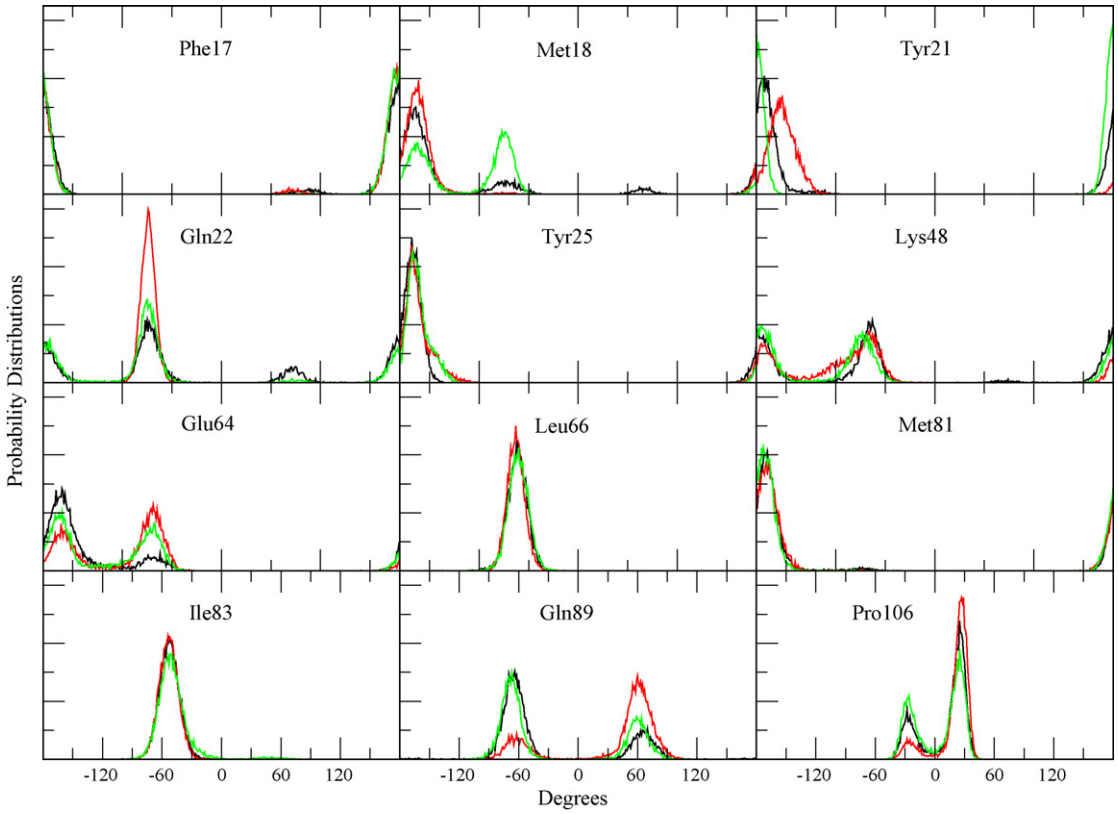

Fig. 5. Probability distributions along the χ angle of selected residues of the receptor-binding region of VEGF. Color scheme is: unbound VEGF (black), VEGF bound to Flt-1_{D2} (red), and VEGF bound to v107 (green).

since it is likely that side-chain rearrangement could improve binding affinity.

3.6. Fluctuations

Experimentally obtained B-factors are available for unbound VEGF and VEGF bound to Flt-1 [12,14]. However, it is not a simple task to compare quantitatively B-factors obtained from different X-ray experiments since the experimental conditions may affect the thermal fluctuations [43]. Thus, in order to understand the effects of binding to the receptor and to the inhibitor on the fluctuations of VEGF, we compared calculated B-factors obtained using the same simulation and averaging conditions. The B-factors of the α-carbon atoms were collected over forty consecutive blocks of 250 ps time length with an interval of 2 ps. Within each block, B-factors were time averaged. B-factors of the two monomers were also averaged. A plot of these blocks shows the time evolution of the B-factors. This can be useful to estimate the convergence of the fluctuations and also to extract conformations in which the same residue has different B-factor values; something which may indicate a transition between conformations. Fig. 6 shows three of these plots: the one of the left corresponding to the free VEGF in solution, the one in the middle corresponding to VEGF bound to Flt-1, and the one in the right corresponding to VEGF bound to v107. A comparison between the three plots show that fluctuations are somewhat higher in the free protein than in the bound systems, mostly in the regions that include residues 10–20 (α-helix next to the binding loops), 35–47 (loop-1 region), 60–70 (loop-2 and part of the adjacent β-strand) and 85–90 (loop-3). The N- and C-terminal regions are also slightly more flexible in the unbound system. RMSD plots are also shown below each B-factor plot in order to give an idea of the time each block was collected. The lower panel (Fig. 6) shows a plot of the averages over all forty blocks. No significant differences are noticeable between the overall averaged B-factors, but it is seen that the order of increasing flexibility is: VEGF_Flt-1_{D2} is less flexible than VEGF_v107 that in turn is less flexible than the free VEGF.

3.7. Collective motions

We previously reported a molecular dynamics study of the unbound VEGF protein in solution, revealing the existence of correlations between the motions of the residues that form the same pole of the dimer [18,19]. A dynamical cross-correlation map (DCCM) was utilized to analyze the collectiveness between the motions of the residues. The DCCM shows whether two residues are moving in the same direction and sense. Positive values on the map indicate correlations and negative values indicate anti-correlations. The map should be symmetric in relation to the diagonal, but for sake of clarity we plotted only the positive values below the diagonal and the negative values above. The values are normalized and range from −1 to 1. Only correlations between −1 and −0.3 and 0.3 and 1 are shown.

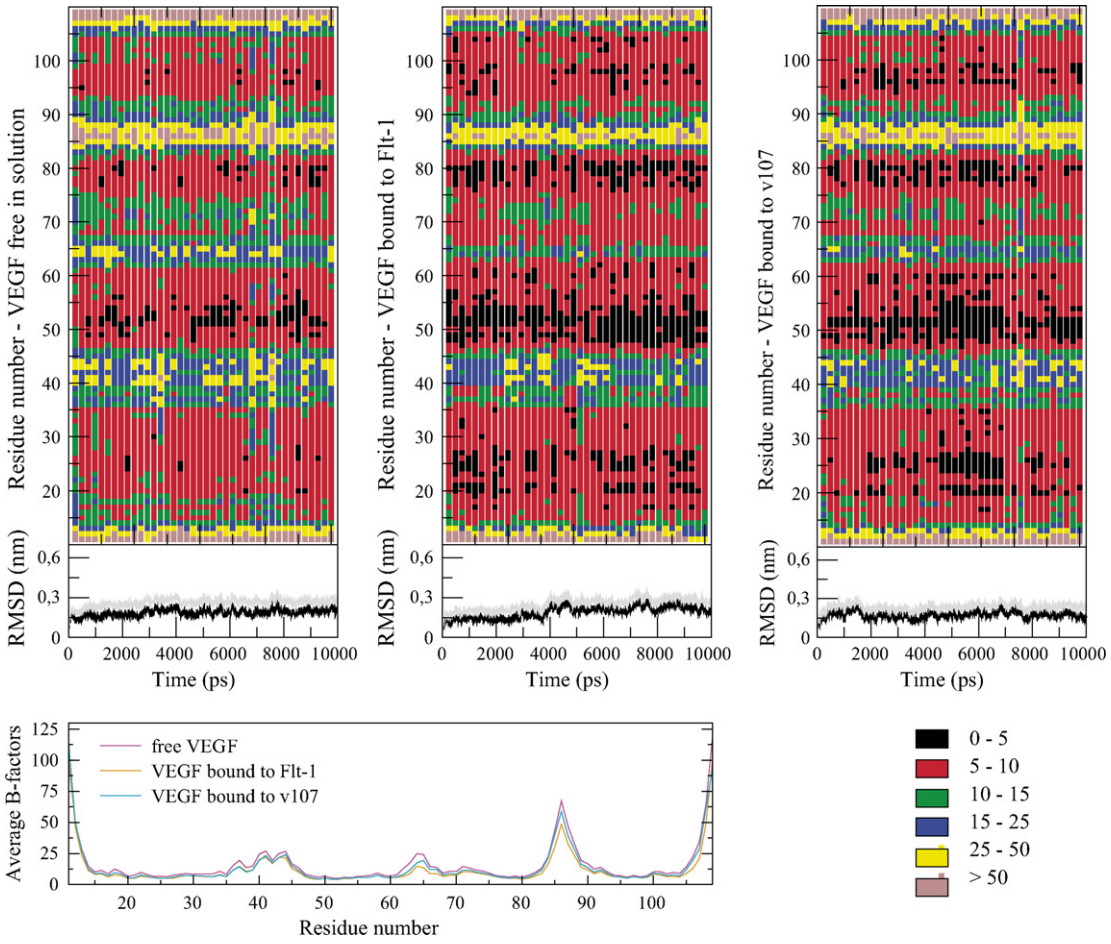

Fig. 6. The three top panels show the time dependence of B-factors collected from consecutive time windows of 250 ps. The panel on the right refers to the unbound VEGF, the panel on the middle refers to VEGF bound to Flt-1_{D2}, and the right panel refers to VEGF bound to v107. Only residues of VEGF are shown and the values are averaged between the two chains. The intensities of the B-factors in the panels are given by the legend on the bottom right. Below each panel lies a RMSD plot to provide an idea of the time each block was collected. In these RMSD plots, the black line refers to α-carbon atom, and the gray line refers to all-atom RMSD. The average of all B-factors blocks are given in the bottom left plot.

Fig. 7 shows the DCCMs for the unbound VEGF [18,19], VEGF_Flt-1_{D2}, VEGF_v107, and VEGF_$v107_{mut}$. In the unbound state (Fig. 7A), relatively strong correlations are observed between the residues that form loop-1 (39–45), loop-2 (62–67), loop-3 (84–89), and some residues of the β-sheet (46–49 and 90–95). In addition, some off-diagonal correlations appears between loops-1 and −3 (39–45 with 84–89), between some residues belonging to different strands of the β-sheet (25–35 with 52–60; 43–50 with 79–83), and between C-terminal and loop-2 (103–109 with 62–67). Comparing the DCCM of the unbound VEGF (Fig. 7A) with those of the bound states (Fig. 7B–D), it is possible to observe a small decrease in the intensities of the correlations. Although minor differences are present, the overall pattern of correlations is very similar.

3.8. Principal component analysis

We previously reported a principal component analysis (PCA) of the unbound VEGF in solution. The results obtained show that the first 10 motional modes account for 99.3% of the total root mean square fluctuations (RMSF). This indicates that the dynamics of VEGF is dominated by the first few components. The first motional mode was shown to be a butterfly like motion, accounting for 72.8% of the total RMSF [18].

The covariance matrix of VEGF bound to Flt-1 and that of VEGF bound to v107 were constructed and diagonalized. To ensure that the configurational sampling of the covariance analysis was sufficient to provide reliable sets of eigenvectors, we compared the root mean square inner products (RMSIP) of the complete space and of the subspace composed by the first 10 eigenvectors (which we considered here as the essential subspace) of subparts of increasing time lengths calculated from two halves of the last 5 ns of each trajectory. Fig. 8 shows the RMSIP for VEGF bound to Flt-1 and for VEGF bound to v107. The solid black line refers to the overlap between eigenvectors obtained for the same system but different trajectory subparts. It serves as a measure of the convergence of the simulations. The top graphs refer to complete space analysis (all eigenvectors) and the bottom ones refer to the defined subspace (first 10 eigenvectors). Simulations are reasonably converged to overlap values of about 0.6

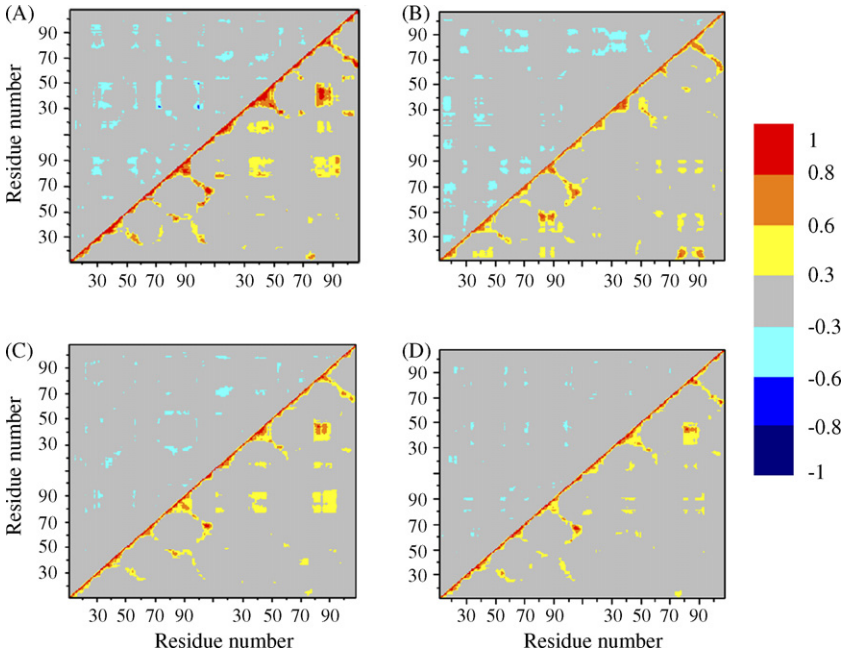

Fig. 7. Dynamical cross-correlation maps (DCCMs). Correlations (positive values) are shown below and anticorrelations (negative values) are shown above the diagonal. The coefficient correlations were calculated by averaging five uninterrupted 1 ns blocks of the last 5 ns of each simulation. Only coefficients higher than 0.30 are shown. (A) Free (unbound) VEGF, (B) VEGF_Flt-1, (C) VEGF_v107, and (D) VEGF_v107$_{mut}$.

(complete space) and 0.5 (subspace). The VEGF bound to v107 shows a somewhat better convergence. It should be mentioned that these overlap values should ideally converge to unity for equilibrated systems. The non-continuous lines refer to the overlap between eigenvectors of bound VEGF (i.e. bound to Flt-1 or v107) with unbound VEGF for the same trajectory subparts. The dotted lines refer to the first 2500 ps and the non-continuous lines refer to the second 2500 ps time subpart. The eigenvectors of VEGF bound to v107 have a good overlap with those of unbound VEGF while the same does not occur for VEGF bound to Flt-1. This indicates that the dynamical behavior of unbound VEGF is close to the dynamical behavior

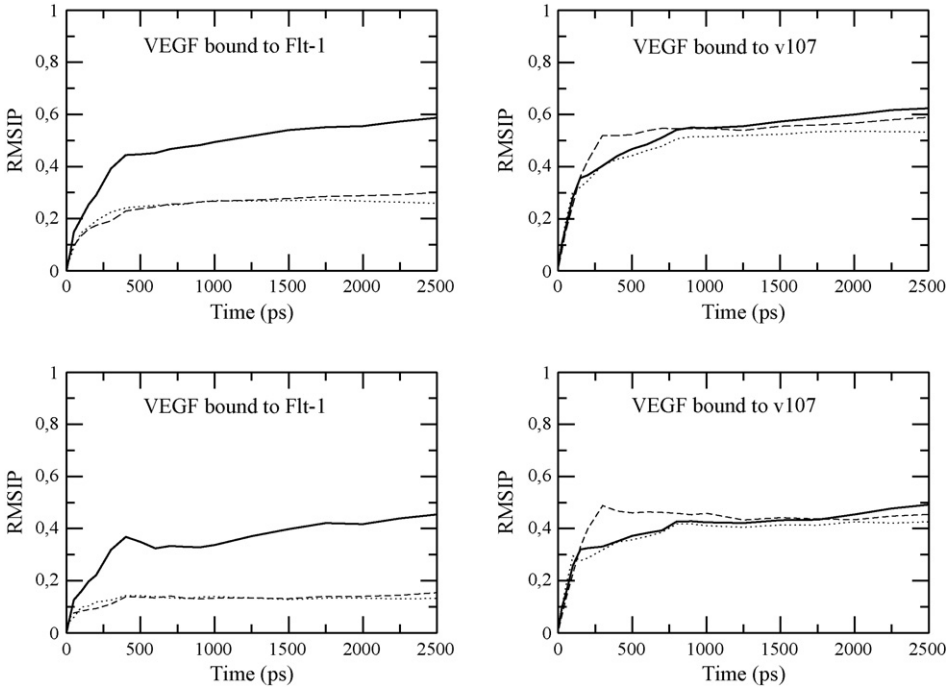

Fig. 8. Root mean square inner products (RMSIP) plots. Top panels show RMSIP over the total space while bottom panels show RMSIP for the subspace which includes the first 10 eigenvectors. The continuous lines are RMSIP between two subparts of 2500 ps of the same trajectory while dotted and non-continuous lines are for the same subpart but different trajectories (i.e. the actual trajectory (VEGF bound to Flt-1 or VEGF bound to v107) with the trajectory of the unbound VEGF).

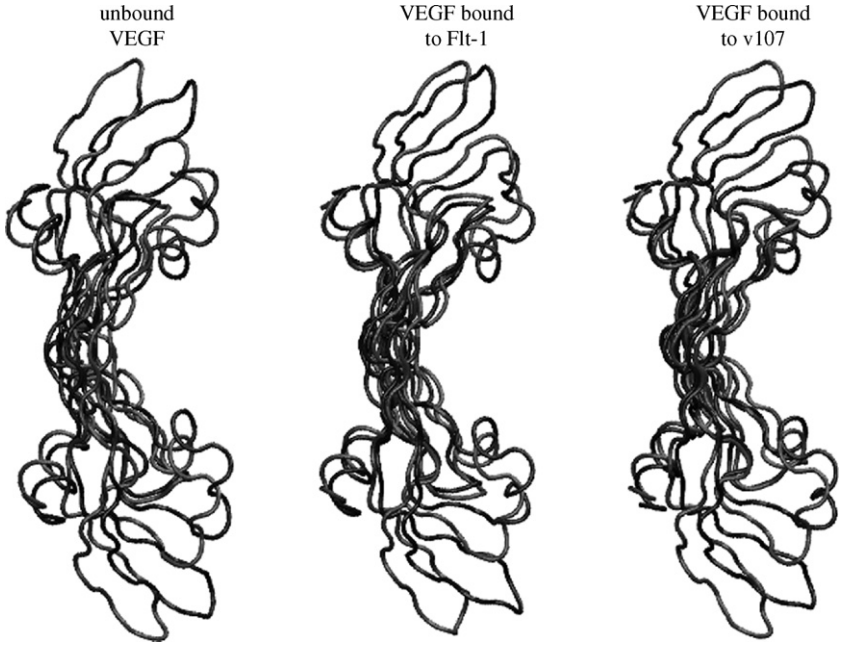

Fig. 9. Extreme structures obtained from the projections of trajectories onto the first eigenvector of PCA.

of VEGF bound to v107. In other words, v107 does not alter significantly the dynamics of VEGF while receptor binding seems to perturb the dynamics of VEGF probably by reducing the correlations. All systems preserved the butterfly like motional mode observed for unbound VEGF as first principal component (Fig. 9). In spite of the overall similarity of the first components, some differences are found in the symmetry of the extreme structures: (i) in the unbound case, a symmetric displacement of the two poles is observed; (ii) in the case of VEGF bound to Flt-1, the upper pole is visibly more closed than the lower pole, indicating some asymmetry in this motion; (iii) in the case of VEGF bound to v107, the motion is also somewhat asymmetric, but it is also detectable a conformational difference between the two poles. This conformational difference between poles of VEGF bound to v107 is also detected in the superimposition of overall structures (Fig. 2), and in the difference in the number of intra-chain hydrogen bonds (Table 2). Together, the above may be a consequence of the different binding orientation between the two copies of v107.

Table 3 lists the minimun values, maximum values, maximum amplitudes, eigenvalues, and percentage of total RMSF of the first eigenvectors for each trajectory. Here, it is noticeable that binding reduces the maximum amplitude reached by the projection onto the first motional mode. Eigenvalue and percentage of the total RMSF are also reduced, suggesting that the dynamics of the unbound protein involves more collectivity. It is possible that the loss of collectivity may affect the configurational entropy of binding.

Table 3
Properties of the first eigenvector of principal component analysis

	Unbound VEGF	VEGF bound to Flt	VEGF bound to v107
Minimum value[a]	−2.214	−1.391	−1.679
Maximum value[a]	1.989	1.706	1.627
Amplitude max[a]	4.202	3.097	3.306
Eigenvalue	0.578	0.303	0.300
Percentage of RMSF	72.8	66.1	65.4

[a] Obtained from the projection of the MD trajectory onto the first motional mode. These values are in nanometers.

4. Conclusions

The biological responses generated by the members of the VEGF family are related to the differential receptor binding characteristics of each growth factor, which are related to minor structural differences. The understanding of how these minor structural differences regulate signal transduction and consequently the biological effects may be the key to the conscious modulation of the process by an intelligent design of promoters and inhibitors. Although great experimental efforts have been made to clarify the structural and functional properties that govern the receptor-binding specificities between these growth factors, the use of theoretical methods may provide important insight to the comprehension of the experimental data, to the proposal of novel experiments and to the rational design of new inhibitors (or promoters).

Herein, we analyze the effects of binding to VEGF regarding three aspects: structure, interactions, and dynamics. In the structure aspect, no breakthrough news was added to what was already demonstrated by experimentalists, that is, no significant changes occur in the structure of VEGF upon binding [14,16]. However, it was shown here that the small peptide inhibitor is able to promote larger modifications in the VEGF average structure and hydrogen bonding pattern than the domain 2 of Flt-1 receptor. In the interaction aspect, per residue energy partition was used to analyze the contribution of each residue of

VEGF on the interactions with Flt-1 and v107. New interactions were identified and described. It seems that specific side-chain interactions play a role in the receptor-binding orientation and recognition. Side-chain distributions were also analyzed which reveal interesting rearrangements that could be explored for future improvement in drug design and docking procedures. Finally, in the dynamics aspect, fluctuations, correlations and principal component analysis (PCA) were investigated. Fluctuations appear not to be strongly affected upon binding, being slightly lower in the bound states as expected. Correlation maps show that the motions of the unbound state are somewhat more collective than those of the bound states. PCA reveals interesting modifications of the dynamical behavior of these systems upon binding. While VEGF bound to Flt-1 seems structurally more similar to unbound VEGF than VEGF bound to v107, the dynamical picture is the opposite. Dynamics of VEGF bound to v107 overlaps very well with that of unbound, while VEGF bound to Flt-1 does not. A strong reduction of the importance of the first eigenvector is also observed from unbound to bound states. It seems that the motions of unbound VEGF are more collective than those of the bound states. Nevertheless, the butterfly-like character of the first eigenvector is still preserved in the bound states. The importance of the collective motions on the configurational entropy of biological processes such as catalysis or receptor binding has been well supported by NMR experiments [44]. However, even if it is still early to hypothesize that the configurational entropy may play a dominant role in VEGF receptor binding, the present work shows that it must be taken into account.

Acknowledgements

The authors would like to thank Dr. Riccardo Baron for fruitful suggestions. We also would like to acknowledge the Brazilian agencies CNPq and FAPERJ for financial support.

References

[1] D.R. Senger, S.J. Galli, A.M. Dvorak, C.A. Perruzzi, V.S. Harvey, H.F. Dvorak, Tumor-cells secrete a vascular-permeability factor that promotes accumulation of ascites-fluid, Science 219 (1983) 983–985.
[2] D.W. Leung, G. Cachianes, W.J. Kuang, D.V. Goeddel, N. Ferrara, Vascular endothelial growth-factor is a secreted angiogenic mitogen, Science 246 (1989) 1306–1309.
[3] D.I.R. Holmes, I. Zachary, The vascular endothelial growth factor (VEGF) family: angiogenic factors in health and disease, Genome Biol. 6 (2005).
[4] P. Carmeliet, Angiogenesis in life, disease and medicine, Nature 438 (2005) 932–936.
[5] X.R. Li, U. Eriksson, Novel VEGF family members: VEGF-B, VEGF-C and VEGF-D, Int. J. Biochem. Cell Biol. 33 (2001) 421–426.
[6] A. Kiba, N. Yabana, M. Shibuya, A set of loop-1 and-3 structures in the novel vascular endothelial growth factor (VEGF) family member, VEGF-ENZ-7, is essential for the activation of VEGFR-2 signaling, J. Biol. Chem. 278 (2003) 13453–13461.
[7] N. Ferrara, H.P. Gerber, J. LeCouter, The biology of VEGF and its receptors, Nat. Med. 9 (2003) 669–676.
[8] H. Gille, J. Kowalski, B. Li, J. LeCouter, B. Moffat, T.F. Zioncheck, N. Pelletier, N. Ferrara, Analysis of biological effects and signaling properties of Flt-1 (VEGFR-1) and KDR (VEGFR-2)—a reassessment using novel receptor-specific vascular endothelial growth factor mutants, J. Biol. Chem. 276 (2001) 3222–3230.
[9] S. Cebe-Suarez, A. Zehnder-Fjallman, K. Ballmer-Hofer, The role of VEGF receptors in angiogenesis; complex partnerships, Cell. Mol. Life Sci. 63 (2006) 601–615.
[10] B.K. McColl, S.A. Stacker, M.G. Achen, Molecular regulation of the VEGF family—inducers of angiogenesis and lymphangiogenesis, Apmis 112 (2004) 463–480.
[11] M.J. Cross, J. Dixelius, T. Matsumoto, L. Claesson-Welsh, VEGF-receptor signal transduction, Trends Biochem. Sci. 28 (2003) 488–494.
[12] Y.A. Muller, H.W. Christinger, B.A. Keyt, A.M. deVos, The crystal structure of vascular endothelial growth factor (VEGF) refined to 1.93 Å resolution: multiple copy flexibility and receptor binding, Structure 5 (1997) 1325–1338.
[13] Y.A. Muller, B. Li, H.W. Christinger, J.A. Wells, B.C. Cunningham, A.M. DeVos, Vascular endothelial growth factor: crystal structure and functional mapping of the kinase domain receptor binding site, in: Proc. Natl. Acad. Sci. U.S.A., 1997, pp. 7192–7197, 94.
[14] C. Wiesmann, G. Fuh, H.W. Christinger, C. Eigenbrot, J.A. Wells, A.M. deVos, Crystal structure at 1.7 Å resolution of VEGF in complex with domain 2 of the Flt-1 receptor, Cell 91 (1997) 695–704.
[15] W.J. Fairbrother, H.W. Christinger, A.G. Cochran, C. Fuh, C.J. Keenan, C. Quan, S.K. Shriver, J.Y.K. Tom, J.A. Wells, B.C. Cunningham, Novel peptides selected to bind vascular endothelial growth factor target the receptor-binding site, Biochemistry 37 (1998) 17754–17764.
[16] B. Pan, B. Li, S.J. Russell, J.Y.K. Tom, A.G. Cochran, W.J. Fairbrother, Solution structure of a phage-derived peptide antagonist in complex with vascular endothelial growth factor, J. Mol. Biol. 316 (2002) 769–787.
[17] C. Wiesmann, H.W. Christinger, A.G. Cochran, B.C. Cunningham, W.J. Fairbrother, C.J. Keenan, G. Meng, A.M. de Vos, Crystal structure of the complex between VEGF and a receptor-blocking peptide, Biochemistry 37 (1998) 17765–17772.
[18] B.A.C. Horta, J.J.V. Cirino, R.B. de Alencastro, Dynamical behavior of the vascular endothelial growth factor: biological implications, Proteins 67 (2007) 517–525.
[19] B.A.C. Horta, J.J.V. Cirino, R.B. de Alencastro, Correction of ‘‘dynamical behavior of the vascular endothelial growth factor: biological implications’’, Proteins 70 (2007) 307–308.
[20] M. Pieren, A.E. Prota, C. Ruch, D. Kostrewa, A. Wagner, K. Biedermann, F.K. Winkler, K. Ballmer-Hofer, Crystal structure of the Orf virus NZ2 variant of vascular endothelial growth factor-E—implications for receptor specificity, J. Biol. Chem. 281 (2006) 19578–19587.
[21] Sybyl, 7.0 Tripos Inc., 1699 South Hanley Rd., St. Louis, Missouri 63144, USA.
[22] E. Lindahl, B. Hess, D. van der Spoel, GROMACS 3.0: a package for molecular simulation and trajectory analysis, J. Mol. Model. 7 (2001) 306–317.
[23] H.J.C. Berendsen, D. Vanderspoel, R. Vandrunen, Gromacs—a message-passing parallel molecular-dynamics implementation, Comput. Phys. Commun. 91 (1995) 43–56.
[24] G.A. Kaminski, R.A. Friesner, J. Tirado-Rives, W.L. Jorgensen, Evaluation and reparametrization of the OPLS-AA force field for proteins via comparison with accurate quantum chemical calculations on peptides, J. Phys. Chem. B 105 (2001) 6474–6487.
[25] H.J.C. Berendsen, J.P.M. Postma, W.F. van Gunsteren, J. Hermans, Interaction models for water in relation to protein hydration, in: B.E. Pullman (Ed.), Intermolecular Forces, Dordrecht, NL, 1981, pp. 331–342.
[26] C.D. Berweger, W.F. Vangunsteren, F. Mullerplathe, Force-field parametrization by weak-coupling—reengineering SPC water, Chem. Phys. Lett. 232 (1995) 429–436.
[27] J. Aqvist, Ion water interaction potentials derived from free-energy perturbation simulations, J. Phys. Chem. 94 (1990) 8021–8024.
[28] B. Hess, H. Bekker, H.J.C. Berendsen, J. Fraaije, LINCS: a linear constraint solver for molecular simulations, J. Comput. Chem. 18 (1997) 1463–1472.
[29] U. Essmann, L. Perera, M.L. Berkowitz, T. Darden, H. Lee, L.G. Pedersen, A smooth particle mesh ewald method, J. Chem. Phys. 103 (1995) 8577–8593.

[30] R.W. Hockney, The potential calculation and some applications, Methods Comput. Phys. 9 (1970) 136–211.
[31] H.J.C. Berendsen, J.P.M. Postma, W.F. Vangunsteren, A. Dinola, J.R. Haak, Molecular-dynamics with coupling to an external bath, J. Chem. Phys. 81 (1984) 3684–3690.
[32] P.H. Hunenberger, A.E. Mark, W.F. Vangunsteren, Fluctuation and cross-correlation analysis of protein motions observed in nanosecond molecular-dynamics simulations, J. Mol. Biol. 252 (1995) 492–503.
[33] W.E. Harte, S. Swaminathan, D.L. Beveridge, Molecular-dynamics of Hiv-1 protease, Proteins Struct. Funct. Genet. 13 (1992) 175–194.
[34] C.A.F. de Oliveira, C.R.W. Guimarães, G. Barreiro, R.B. de Alencastro, Human cytomegalovirus protease: why is the dimer required for catalytic activity? J. Chem. Theory Comput. 3 (2007) 278–288.
[35] K. Tai, T.Y. Shen, U. Borjesson, M. Philippopoulos, J.A. McCammon, Analysis of a 10-ns molecular dynamics simulation of mouse acetylcholinesterase, Biophys. J. 81 (2001) 715–724.
[36] M.A. Starovasnik, H.W. Christinger, C. Wiesmann, M.A. Champe, A.M. de Vos, N.J. Skelton, Solution structure of the VEGF-binding domain of Flt-1: comparison of its free and bound states, J. Mol. Biol. 293 (1999) 531–544.
[37] A.D. McLachlan, Rapid comparison of protein structures, Acta Crystallogr. Sect. A 38 (1982) 871–873.
[38] A.C.R Martin, PROFIT V2.5 (2005), http://www.bioinf.org.uk/software/profit/.
[39] M. Heinig, D. Frishman, STRIDE: a web server for secondary structure assignment from known atomic coordinates of proteins, Nucleic Acids Res. 32 (2004) W500–W502.
[40] B.A. Keyt, H.V. Nguyen, L.T. Berleau, C.M. Duarte, J. Park, H. Chen, N. Ferrara, Identification of vascular endothelial growth factor determinants for binding KDR and FLT-1 receptors—generation of receptor-selective VEGF variants by site-directed mutagenesis, J. Biol. Chem. 271 (1996) 5638–5646.
[41] L.P. Aiello, E.A. Pierce, E.D. Foley, H. Takagi, H. Chen, L. Riddle, N. Ferrara, G.L. King, L.E.H. Smith, Suppression of retinal neovascularization in vivo by inhibition of vascular endothelial growth-factor (VEGF) using soluble VEGF-receptor chimeric proteins, in: Proc. Natl. Acad. Sci. U.S.A., 1995, pp. 10457–10461, 92.
[42] W. Humphrey, A. Dalke, K. Schulten, VMD: visual molecular dynamics, J. Mol. Graph. 14 (1996) 33–38.
[43] H. Frauenfelder, G.A. Petsko, D. Tsernoglou, Temperature-dependent X-ray-diffraction as a probe of protein structural dynamics, Nature 280 (1979) 558–563.
[44] V.A. Jarymowycz, M.J. Stone, Fast time scale dynamics of protein backbones: NMR relaxation methods, applications, and functional consequences, Chem. Rev. 106 (2006) 1624–1671.